http://dx.doi.org/10.1016/j.jmb.2012.07.022 J. Mol. Biol. (2012) 423, 284–293

Contents lists available at www.sciencedirect.com

Journal of Molecular Biology

journal homepage: http://ees.elsevier.com.jmb

COMMUNICATION

Investigating Terephthalate Biodegradation: Structural Characterization of a Putative Decarboxylating *cis*-Dihydrodiol Dehydrogenase

Jasleen Bains[1]†, Jeremy E. Wulff[2] and Martin J. Boulanger[1]*

[1]*Department of Biochemistry and Microbiology, University of Victoria, PO Box 3055 STN CSC, Victoria, BC, Canada V8W 3P6*
[2]*Department of Chemistry, University of Victoria, PO Box 3055 STN CSC, Victoria, BC, Canada V8W 3P6*

Received 29 May 2012;
received in revised form
24 July 2012;
accepted 28 July 2012
Available online
11 August 2012

Edited by G. Schulz

Keywords:
Burkholderia xenovorans LB400;
tph pathway;
cis-dihydrodiol;
TphB;
zinc

As a highly coveted precursor molecule, terephthalate (Tph) continues to be used extensively for the production of polyethylene Tph bottles, polyester films, and textile fibers worldwide. Based on its detrimental physiological effects, Tph is now recognized as a serious environmental pollutant. While amenable to biodegradation and, in fact, traditionally neutralized by aerobic microbiological processes, our current lack of understanding of the enzymatic degradation of Tph at the molecular level presents a major impediment in the development of robust bioremediation strategies. The biodegradation of Tph proceeds through a single metabolic intermediate (a *cis*-dihydrodiol), which is subsequently converted to the end product (protocatechuate) by a decarboxylating *cis*-dihydrodiol dehydrogenase (TphB). Using iodide single-wavelength anomalous dispersion, we report the first structural characterization of TphB to 1.85 Å resolution. Contrary to prior speculations, a fluorescent scan unambiguously shows that TphB coordinates Zn^{2+} and not Fe^{2+}. The molecular architecture of TphB provides a rationale to the primary-level divergence observed between TphB and other *cis*-dihydrodiol dehydrogenases while explaining its intriguingly close evolutionary clustering with non-dihydrodiol dehydrogenases belonging to the isocitrate/isopropylmalate family of enzymes. Sequence and structural analyses reveal a putative substrate-binding pocket proximal to the bound Zn^{2+}. *In silico* substrate modeling in this putative binding pocket suggests a mechanistic sequence relying on H291, K295, and Zn^{2+} as core mediators of catalytic turnover. Overall, this study reveals novel structural and mechanistic insights into a decarboxylating *cis*-dihydrodiol dehydrogenase that mediates one of the two catalytic steps in the biodegradation of the environmental pollutant Tph.

**Corresponding author.* E-mail address: mboulang@uvic.ca.

† Currently a Natural Sciences and Engineering Research Council Postdoctoral Fellow at ABM, Richmond, BC, Canada.

Abbreviations used: LB400, *Burkholderia xenovorans* LB400; Tph, terephthalate; TphB, terephthalate 1,2-*cis*-dihydrodiol dehydrogenase; SEC, size-exclusion chromatography; EC, Enzyme Commission; IDH, isocitrate dehydrogenase; PDB, Protein Data Bank; EDTA, ethylenediaminetetraacetic acid.

0022-2836/$ - see front matter

Introduction

Terephthalate (Tph), isophthalate, and phthalate are nonreactive aromatic compounds (benzene dicarboxylate isomers) that can enter the environment from industrial or natural sources.[1,2] The production of purified Tph alone ranks among the top 50 chemicals manufactured in the world, which translates to high levels of Tph and other organic contaminants (acetate, benzoate, and *p*-toluate) as waste products.[3] Based on their wide-ranging adverse effects on animal cells,[4–11] as well as considering the decades of global industrial use as plasticizers and polymers, these aromatic isomers are now recognized as serious and ubiquitous pollutants.[4,12] With microbial biodegradation as the primary portal for mediating the bio-friendly and cost-effective neutralization of these pollutants, it is imperative that such bioprocesses are investigated in sufficient detail to enable design and implementation of improved bioremediation strategies. While some studies have indeed been conducted relevant to these benzene dicarboxylate isomers,[1,13,14] our understanding of the biodegradation processes involved, especially for Tph and isophthalate, remains limited.[15–17] Furthermore, the biodegradation of Tph (1,4-dicarboxybenzene) also holds promise for an alternative bio-friendly application that entails use of Tph as a starting compound for the production of biodegradable 2-pyrone-4,6-dicarboxylate polyamides and polyesters.[18–20]

Several microorganisms have demonstrated the capability to degrade Tph.[21–24] Studies at the genetic and biochemical level encompass members from both the Gram-positive (*Rhodococcus* sp. strain DK17,[25] *Rhodococcus* sp. strain RHA1[26]) and Gram-negative (*Comamonas testosteroni* T-2,[2,27] *C. testosteroni* YZW-D,[28] *Comamonas* sp. strain E6,[29] and *Delftia tsuruhatensis* strain T7[30]) bacteria. To probe Tph degradation from a new microbe, and one that can be effectively and holistically harnessed for bioremediation applications, owing to an outstanding repertoire of 11 "central aromatic" and 20 "peripheral aromatic" pathways,[31] we choose to focus our attention on *Burkholderia xenovorans* LB400 (LB400 hereinafter). In addition to a putative *tph* operon (functionally uncharacterized), LB400's uniquely rich metabolic inventory endows this bacterium with the capability to degrade various environmental toxins, including, but not limited to, nitro-aromatics,[32] polycyclic aromatic hydrocarbons,[33] and chlorinated aromatic compounds.[34–36] A closer, comparative analysis of both the organization and the nucleotide sequences of the protein and enzymatic components within the putative *tph* operon confirms its annotation in the database. The *tph* operon in LB400 encodes a regulatory protein, a transport protein, the large and small subunit of a putative dioxygenase (TphA1A2), a putative *cis*-dihydrodiol dehydrogenase (TphB), and a putative reductase (TphA3).

The gene products of the *tph* operon catalyze the conversion of Tph into protocatechuate (Fig. 1a) via the only pathway intermediate *cis*-dihydrodiol [variously referred to in the literature as either *cis*-4,5-dihydroxycyclohexa-1(6),2-diene-1,4-dicarboxylate or (3*R*,4*S*)-3,4-dihydroxycyclohexa-1,5-diene-1,4-dicarboxylic acid]. It is noteworthy that dihydrodiols are key, nonaromatic intermediates formed during the metabolism of aromatic compounds in both prokaryotes and eukaryotes and represent an activated form of the parent benzenoid nucleus. Typically, dihydrodiols with *cis* stereochemistry[38] (as mentioned above with respect to the *tph* pathway) are formed during microbial aromatic metabolism, while *trans*-dihydrodiols are often generated during the metabolism of aromatic compounds by the mammalian liver.[39,40] A dedicated set of mostly stereo-selective dehydrogenases [Enzyme Commission (EC) 1.3.1.X] are employed to catalyze the NAD(P)$^+$-dependent oxidation of *trans*-dihydrodiols and, in select cases, an oxidative decarboxylation of *cis*-dihydrodiols. While *trans*-dihydrodiol dehydrogenases have been implicated in the metabolism of endogenous steroids, prostaglandins,[41] and xenobiotics[42] and suggested as prognostic markers for certain cancers,[43] the *cis*-dihydrodiol dehydrogenases are fundamental to the microbial biodegradation of both natural and xenobiotic aromatic compounds.

The *cis*-dihydrodiol dehydrogenase from the *tph* pathway (Q13RP4), variously identified as Tph 1,2-*cis*-dihydrodiol dehydrogenase, 1,2-dihydroxy-3,5-cyclohexadiene-1,4-dicarboxylate dehydrogenase, or DCD dehydrogenase (TphB hereinafter), is one such enzyme that catalyzes the oxidative decarboxylation of *cis*-4,5-dihydroxycyclohexa-1(6),2-diene-1,4-dicarboxylate to protocatechuate (Fig. 1a). Based on the reaction catalyzed, TphB delineates its own EC niche (EC 1.3.1.53) within the existing repertoire of *cis*-dihydrodiol dehydrogenases, most of which have been studied with respect to the biodegradation of benzene, toluene, ethylbenzene, naphthalene, benzoate, *p*-chlorotoluene, and 5-amino-4-chloro-2-phenyl-3-(2*H*)-pyridazinone.[44] Interestingly, TphB represents one of the four *cis*-dihydrodiol dehydrogenases that have, in addition, a decarboxylating component to their reaction chemistry and the only one that funnels into protocatechuate *versus* the relatively more popular central metabolite catechol/substituted catechol. Currently, representatives from only two sub-subclasses (EC 1.3.1.28[45] and EC 1.3.1.56[46]) of *cis*-dihydrodiol dehydrogenases stand structurally characterized, which warrants further investigation of these physiologically important group of enzymes. Therefore, with an aim to investigate the molecular basis of Tph degradation

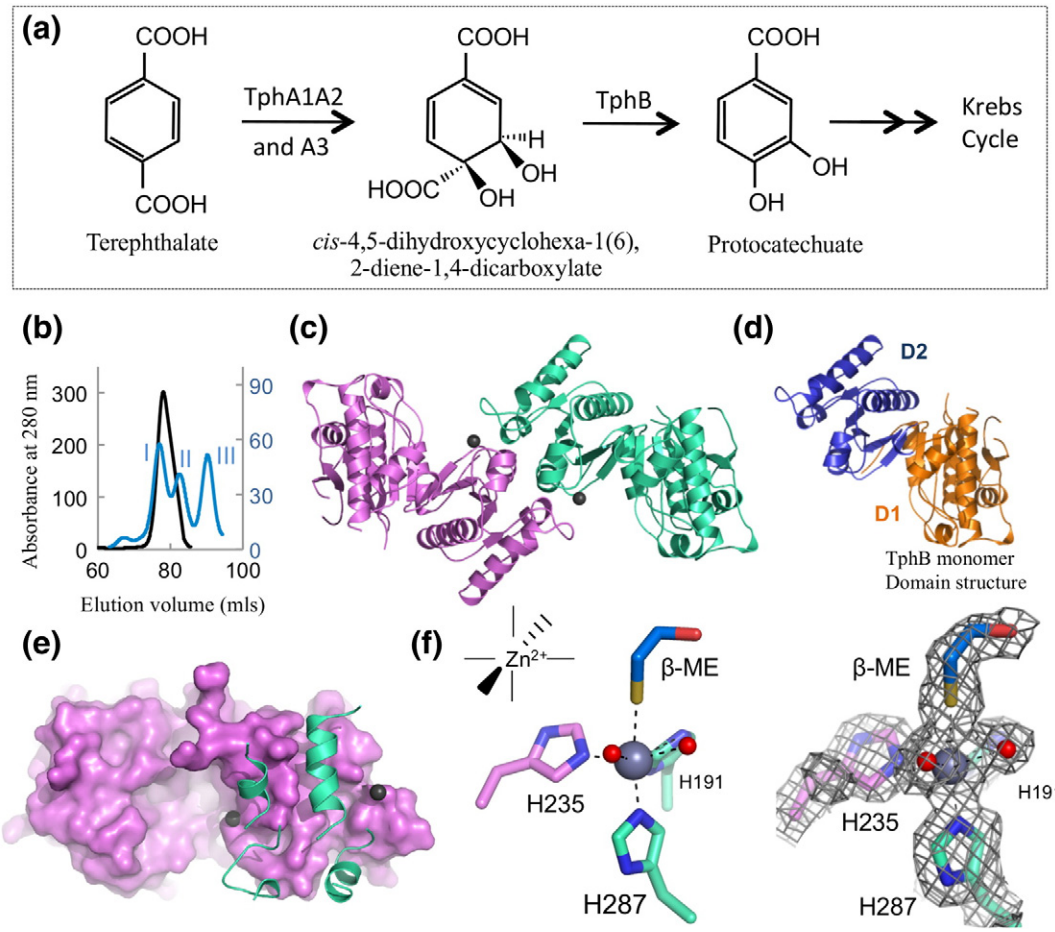

Fig. 1. (a) Schematic for the *tph* pathway that begins with Tph and terminates with the formation of protocatechuate, which is eventually metabolized into Krebs cycle intermediates. (b) The elution profile of TphB reveals a stable dimeric conformation with an approximate molecular mass of 73 kDa. The protein peaks in the standard curve refer to conalbumin (I—75 kDa), ovalbumin (II—45 kDa), and carbonic anhydrase (III—29 kDa). (c) The TphB dimer shown in violet (chain A) and lime green (chain B). (d) The subdomain division of the TphB monomer. Shown in orange is the N-terminal subdomain D1 while shown in blue is the C-terminal subdomain D2. (e) Surface topology of the dimeric interface for TphB that is largely mediated by α-helices. (f) Left: Chemical representation of an octahedral geometry alongside a ball-and-stick representation of the metal site with Zn^{2+} shown as a gray sphere, waters as red spheres, a molecule of β-mercaptoethanol, and the three histidine residues contributed by both the monomers in TphB. Right: $2F_o - F_c$ electron density map contoured at 1σ for Zn^{2+} and its coordinating ligands. All the figures have been generated using PyMOL.[37]

as well as explore *cis*-dihydrodiol dehydrogenases in general, we report the 1.85-Å-resolution crystal structure of TphB from LB400 solved using iodide phasing. Our structure is the first reported for a TphB and reveals mechanistic insight into this important group of enzymes.

Results and Discussion

Homodimerization of TphB creates the requisite scaffold for metal binding

To investigate the structural basis of Tph degradation, we recombinantly produced TphB in *Escherichia coli* BL21 (DE3) and purified the protein to homogeneity using nickel affinity chromatography and size-exclusion chromatography (SEC). The elution profile from the SEC column revealed a stable homodimeric quaternary structure with an overall molecular weight of approximately 73 kDa (Fig. 1b) similar to that observed for the only other comprehensively, biochemically characterized TphB homolog from *C. testosteroni* T-2.[27] Crystallization of TphB revealed a dimer in the asymmetric unit of *C*2221 with the native dimeric configuration generated by a 2-fold noncrystallographic axis of symmetry (Fig. 1c). A complexation significance score of 1.00 indicates that the buried interface is energetically sufficient to promote assembly into a dimeric quaternary conformation. The buried surface area within the dimeric interface (~1200 Å^2) accounts for approximately 10% of the total surface area and is

comparable to other known dehydrogenases.[47] The final model was refined to a resolution of 1.85 Å, starts at residue 9 for chain A and at residue 8 for chain B, and includes an unmodeled loop region for chain A (residues 38–49) and chain B (residues 38–48) before terminating with residue 347 in both chains. Data collection and model refinement statistics are presented in Supplementary Table 1.

Overall, the TphB monomer adopts an alpha–beta fold that comprises an inner core formed by an extended, mixed β-sheet comprising 11 β-strands. The β-sheet is twisted along its longitudinal axis and sandwiched between a total of 10 α-helices. Despite no clear demarcation for domain structure at the level of primary sequence, the structure of the TphB monomer reveals two subdomains, D1 (residues 1–167; 306–349) and D2 (residues 168–305) (Fig. 1d). The D1 and D2 subdomains adopt an extended V-shaped structure that pivots in the middle at the two antiparallel β-strands, one from each subdomain. The N and C termini are encompassed within D1 while the dimeric interface is formed through the interactions between the D2 subdomains of the TphB monomers.

During refinement, $2F_o - F_c$ electron density maps of native TphB revealed two symmetry-related peaks that were too large for water molecules and suggestive of transition metal ions. Coincidentally, a previous characterization of a TphB homolog revealed that ethylenediaminetetraacetic acid (EDTA) inhibited enzyme activity.[27] Based on the coordination geometry, type of interacting side-chain moieties, and associated topological features, zinc appeared to be a likely candidate. A source of ambiguity, however, arose from previous work on the same (aforementioned) TphB homolog[27] where Fe^{2+} were shown to have a stimulatory effect on enzyme activity alongside a restoration effect following treatment with EDTA. To establish the nature of the bound metal, we performed a K-edge fluorescence scan on the TphB crystal for both Fe^{2+} and Zn^{2+}. While no signal was detected at the K-edge of Fe^{2+}, a clear fluorescence peak was observed at the Zn^{2+} K-edge consistent with Zn^{2+} bound to TphB.

The two Zn^{2+} are positioned at the surface and bulk solvent-exposed facet of the dimer interface and coordinated by the $N^{\varepsilon 2}$ imidazole nitrogens of H191 and H287 from one monomer and H235 from the second monomer (Fig. 1f; note that residue numbering is offset by +3 with respect to native sequence of TphB due to the presence of three additional residues remaining from thrombin cleavage). Two water molecules and a molecule of β-mercaptoethanol complete the octahedral coordination sphere of each Zn^{2+} for the native data set solved in $C222_1$ (Fig. 1f). The distances between the Zn^{2+} and the coordinating nitrogen, oxygen, and sulfur range from 2.1 to 2.8 Å. It is noteworthy that pure structural metal sites comprise four protein ligands with no bound water molecule(s), suggesting that the Zn^{2+} sites in TphB are catalytic.[48] Furthermore, treatment with EDTA did not compromise the structural integrity of TphB as determined by the elution profile on a size-exclusion column. With the two Zn^{2+} sites formed at the dimer interface, it appears that dimerization is necessary to generate a functional enzyme.

Substrate-specific reaction chemistry likely necessitates the presence of the divergent D2 domain

All known *cis*- and *trans*-dihydrodiol dehydrogenases are categorized as one of 15 EC 1.3.1 sub-subclasses. Other than the *trans*-dihydrodiol dehydrogenases belonging to EC 1.3.1.20, which have been the most extensively structurally characterized,[49] structures for representative members (2,3-dihydro-2,3-dihydroxybenzoate dehydrogenase[45] and *cis*-2,3-dihydro-2,3-dihydroxybiphenyl dehydrogenase[46,50]) from only two other categories (EC 1.3.1.28 and EC 1.3.1.56, respectively) have been reported, underscoring our limited understanding of this important group of enzymes. Structural comparison between TphB and the previously characterized dihydrodiol dehydrogenases (Fig. 2a–c) reveals a pattern whereby the homology is confined to the D1 subdomain. While low sequence identity can, in part, explain this observation, the presence of a completely divergent D2 subdomain relative to these dihydrodiol dehydrogenases is intriguing. However, a DALI[51] structural homology search confirms our initial BLAST[53] analysis, indicating that TphB closely resembles (spanning both the subdomains) dehydrogenases that act on non-dihydrodiol substrates (Fig. 2d) and are members of the 3-isopropylmalate and isocitrate dehydrogenase (IDH) superfamily of enzymes.

Specifically, a 4-hydroxy threonine-4-phosphate dehydrogenase from E. coli[47] [Protein Data Bank (PDB) code 1PS6; IDH member] displays the highest *Z* score of 31.6 (DALI score) with an r.m.s.d. of 4.1 Å over 328 C^{α} atoms with 27% identity. Currently, the PDB lists five crystal structures for 4-hydroxy threonine-4-phosphate dehydrogenases (2HI1, putative *Salmonella typhimurium*; 1YXO, *Pseudomonas aeruginosa*; 3LXY, *Yersinia pestis*; CO92 and 3TSN, *Campylobacter jejuni*; and 1PS6/1PS7/1PTM, *E. coli*) of which only 1PS6/1PS7/1PTM appear in a published journal.[47] In order to assess the phylogenetic categorization of TphB (Q13RP4) with regard to both the dihydrodiol and non-dihydrodiol dehydrogenases, a phylogenetic tree was constructed (Fig. 2e). Based on the availability of annotated amino acid sequences, our analysis includes members from 8 of the 15 categories for the dihydrodiol dehydrogenases ranging from 248 to 400 amino acids in length as well as one representative member from 4-hydroxythreonine-4-phosphate dehydrogenase, 3-isopropylmalate dehydrogenase, and isocitrate dehydrogenase. Among the representative members displayed in Fig. 2e, the non-dihydrodiol

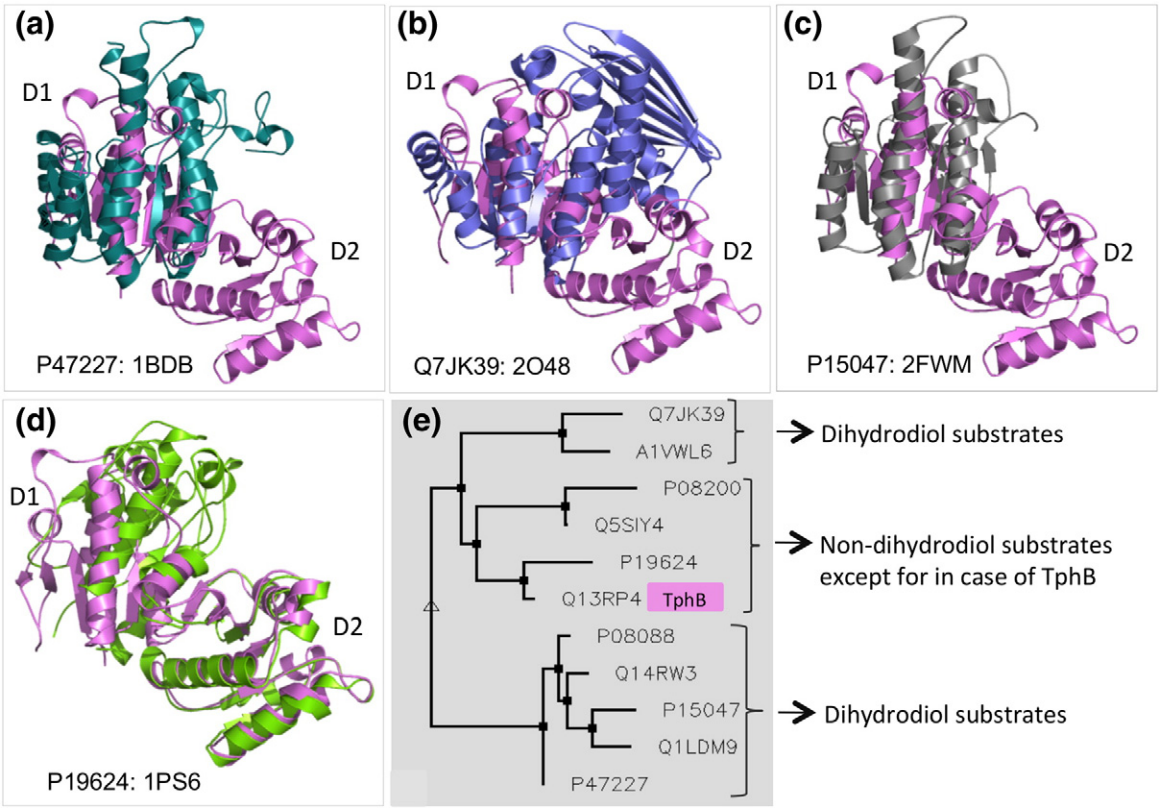

Fig. 2. Structural overlay of TphB monomer (violet) with (a) *cis*-2,3-dihydrobiphenyl-2,3-diol dehydrogenase (EC1.3.1.56), PDB code 1BDB; (b) *trans*-1,2-dihydrobenzene-1,2-diol dehydrogenase (EC1.3.1.20), PDB code 2O48; (c) 2,3-dihydro-2,3-dihydroxybenzoate dehydrogenase (EC 1.3.1.28), PDB code 2FWM; and (d) 4-hydroxy threonine-4-phosphate dehydrogenase (EC 1.1.1.262), PDB code 1PS6 on the DALI server.[51] The statistics for these overlays are as follows: *Z* score: 3.5, aligned C^{α} atoms: 126, r.m.s.d.: 3.8 Å with 13% identity for 1BDB. *Z* score: 3.2, aligned C^{α} atoms: 99, r.m.s.d.: 3.8 Å with 14% identity for 2O48. *Z* score: 3.7, aligned C^{α} atoms: 116, r.m.s.d.: 3.7 Å with 9% identity for 2FWM. *Z* score: 31.6, aligned C^{α} atoms: 328, r.m.s.d.: 4.1 Å with 27% identity for 1PS6. (e) A phylogenetic tree constructed using the program MultAlin.[52] Protein accession codes are listed.

and dihydrodiol dehydrogenases are well segregated with the exception of TphB that clusters with the non-dihydrodiol dehydrogenases.

It is noteworthy that only four types of dihydrodiol dehydrogenases (EC 1.3.1.25, 1.3.1.53, 1.3.1.67, and 1.3.1.68) catalyze reactions that involve both a dehydrogenation and a decarboxylation event of which TphB (1.3.1.53) reported in this article is the first to be structurally characterized. Like TphB, all structurally related non-dihydrodiol dehydrogenases have an obligate requirement for a metal ion. This could explain the evolutionary requirement for a D2 subdomain-like substructure, which in this case provides the appropriate scaffold to accommodate the metal ion. The latter explanation is supported by the observation that the 4-hydroxythreonine-4-phosphate dehydrogenase, which shares the highest similarity, has a nearly identical Zn^{2+} site with TphB. Furthermore, the three other 4-hydroxythreonine-4-phosphate dehydrogenases (unpublished structures) coordinate a Ni^{2+} or Mg^{2+} (3TSN, 3LXY, and 1YXO, respectively) alongside the relatively more divergent IDHs that are known to coordinate either a Mg^{2+} or Mn^{2+} as the metal cofactor. It is unknown if the other three mechanistic homologs of TphB (among the dihydrodiol dehydrogenases) require a metal ion, although based on the length of their primary sequence and the associated distant phylogeny (Q1LDM9) with TphB, it is unlikely that they possess a similar D2 subdomain. Thus, it appears that the D2 subdomain in TphB is designed to support a reaction mechanism with a requirement for metal-based catalytic chemistry.

A conserved, metal proximal site exhibits favorable chemical topology to bind the native substrate

Structural comparisons with TphB homologs combined with the identification of the catalytic Zn^{2+} site enabled the localization and characterization of the active-site structure in TphB, which is niched within the cradle-like surface topology

formed at the subdomain interface (Fig. 3a; black square boxes) and extending to the metal ion coordinated at the dimeric interface. Sequence alignment between TphB from LB400 and TphB from other prokaryotes supports an important role for this region with the clustering of highly conserved residues (Fig. 3b and c). To further aid in the demarcation of the active site, we generated an electrostatic surface of TphB (Fig. 3d), which revealed a large basic patch extending from the bound Zn^{2+} capable of complementing the negative charge of the TphB substrate.

Overall, the active-site pocket is substantially solvent exposed (Fig. 4a), which is not surprising considering the highly polar nature of the native substrate (Fig. 1a). However, three leucine residues (L176, L178, and L190; Fig. 4b) define one face of this putative binding pocket forming a hydrophobic region capable of accommodating the nonpolar carbon backbone of the dihydrodiol substrate and the lipophilic part of the $NAD(P)^+$ cofactor. The proximal GHGSG sequence in TphB (Fig. 4a and b), which closely resembles the phosphate binding consensus sequence GXGXXG, likely participates in ensuring proper juxtaposition of the $NAD(P)^+$ cofactor for hydride transfer. A lysine (K295) that sits atop this shallow pocket is the likely candidate for coordinating the carboxylate that remains unchanged between the substrate and product (Fig. 4a and b). The $N^{\delta 1}$ atoms of two out of the three Zn^{2+} coordinating histidines, H235 and H287 (one from each monomer), are involved in hydrogen-bonding interactions with the $O^{\delta 1}$ of E238 and $O^{\delta 1}$ of D288, respectively (Fig. 4a). These interactions likely serve to ensure correct orientation for these histidine residues as also suggested for the analogous histidine–aspartate interaction observed in 4-hydroxythreonine-4-phosphate dehydrogenase.[47] It is noteworthy that equivalents of all these residues are, to the best of our knowledge, absolutely conserved in Tph 1,2-*cis*-dihydrodiol dehydrogenases (sequence alignment; Supplemental Data). Considering the stereochemistry and redox potential of the native substrate of TphB and the need for correct spatial juxtaposition to enable metal-mediated reaction chemistry, we predict that TphB will be highly specific for its native substrate.

Proposed reaction mechanism

The current theory for the mechanism of TphB-mediated conversion of the *cis*-dihydrodiol pathway intermediate into protocatechuate includes an initial dehydrogenation event followed by decarboxylation.[2,28] Due to the lack of commercial availability of the native substrate to support co-crystallization, we constructed an *in silico* model of the enzyme–substrate complex, taking into account all of the residues of the putative active site (Fig. 4c). To assist in the design of the model, we first examined several small-molecule structures in the Cambridge Structural Database where Zn^{2+} was bound to α-hydroxy acid or α,β-dihydroxy acid functions. This search

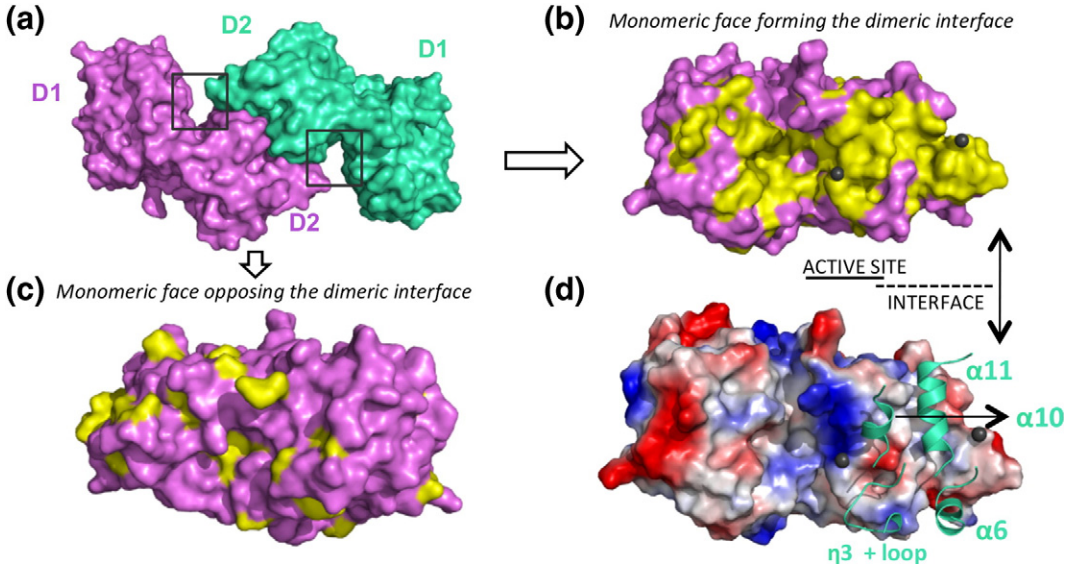

Fig. 3. (a) An overview of the active-site localization in TphB positioned at the inter-subdomain interface, which can be distinguished by a groove-like surface topology (indicated by black square boxes). (b and c) An illustration of sequence conservation (yellow) mapped on to TphB structure, where (b) denotes the highly conserved (represented as yellow) dimer face while (c) depicts the more divergent surface opposing the dimer interface. Note that the color scheme employed for depicting the sequence conservation is purely arbitrary. (d) Electrostatic representation of the dimer interface.

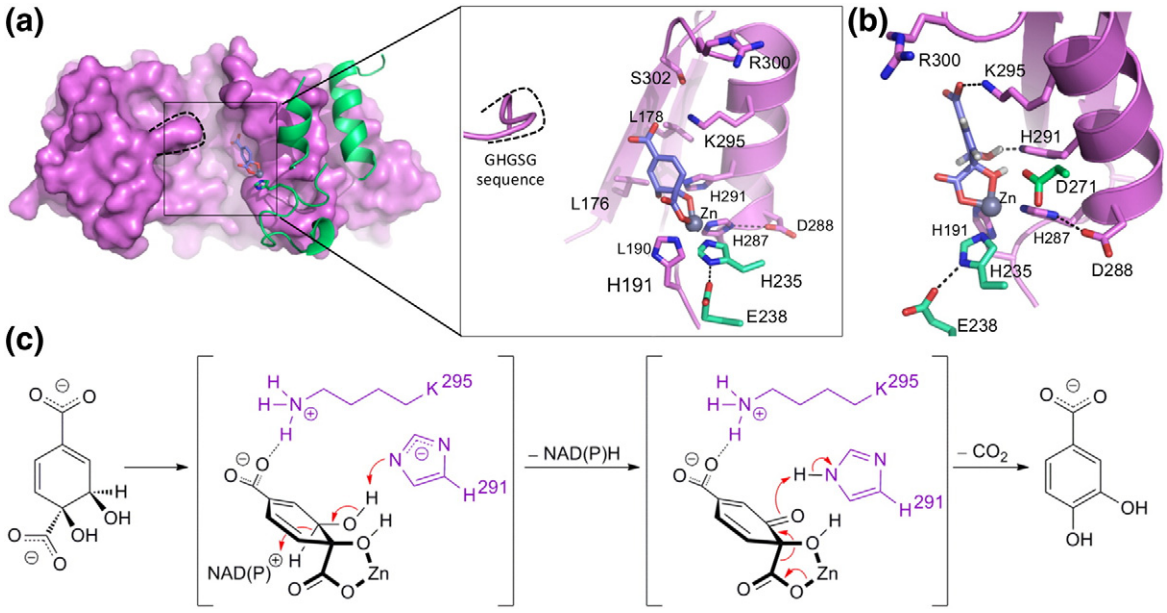

Fig. 4. (a) An overview of the location of the proposed active site highlighting the modeled native substrate that is in close proximity to the zinc site. A close-up view of the active site showcasing key residues that form this active site as well as those likely involved in catalysis; the black dashes indicate the GHGSG sequence tag in TphB, which bears semblance to the consensus sequence for binding the phosphate of the coenzyme. (b) A depiction of a rotated view of (b) to highlight the interaction between the modeled native substrate (with hydrogens shown in this case) and both H291 and K295. (c) A mechanistic schematic highlighting the roles of Zn^{2+}, H291, and K295 in catalysis.

revealed a marked preference for α-hydroxy acids to bind in a bidentate fashion, using one oxygen of the carboxylate together with the alcoholic oxygen. α,β-Dihydroxy acids bound with a qualitatively similar geometry; other possible binding modes (e.g., bidentate coordination through both oxygen atoms of the carboxylate group or tridentate coordination through the carboxylate and both alcohols) were not represented in the database.

We therefore constructed our model by beginning with a bidentate coordination of the α-hydroxy acid function in the *cis*-dihydrodiol intermediate to the tris-histidine–zinc complex (Fig. 4b and c). Geometry optimization by both molecular mechanics (MMFF) and semiempirical (PM3) methods placed the vinylic carboxylate function in close proximity to K295, as predicted from our preliminary examination of the active-site geometry. It is also possible that R300 plays a role in binding the distal carboxylate, but this would require a substantial rearrangement of the arginine side chain.

The geometry-optimized model placed the non-coordinated alcohol in close proximity to H291. Intriguingly, when this histidine was modeled in its deprotonated state, geometry optimization (Fig. 4c) resulted in a very close contact (1.8 Å) between the $N^{\varepsilon 2}$ imidazole nitrogen of H291 and the proton of the β-hydroxyl group. Moreover, this "protic" hydrogen is in an almost perfectly antiperiplanar orientation relative to the "hydridic" hydrogen that must be expelled as part of the dehydrogenation event. In addition, the hydridic hydrogen points into the open cavity of the putative active site, where it would be well placed for delivery to bound $NAD(P)^+$. Based on these calculations, we hypothesize that the mechanism follows the process outlined in Fig. 4c where dehydrogenation promoted by H291 results in the transient formation of a β-keto acid, which would rapidly lose CO2 to generate protocatechuate and promote de-coordination of the active-site Zn^{2+}, thereby allowing the enzyme to return to its catalyst-ready state. Aside from orienting the substrate, which seems to be the primary role of Zn^{2+}, the modeling data suggest that having one hydroxyl group bound to Zn^{2+} (Fig. 4b and c) greatly improves hydrogen bonding to the neighboring alcohol in the substrate. This effect is due to optimized geometry (binding of the OH to the zinc requires that the proton point back toward the unbound alcohol) and electrochemistry (binding of the OH to the Zn^{2+} should also lower the pK_a of the bound functional group). The resulting increase in intramolecular hydrogen bonding should enhance the acidity of the unbound alcohol, which in turn will facilitate the reaction.

Conclusions

Here, we report the three-dimensional structure of TphB, the first of a decarboxylating dehydrogenase

to act on a *cis*-dihydrodiol substrate structural characterization of the dehydrogenase that mediates the second and final step in the biodegradation pathway of the major environmental pollutant Tph. A structural comparison of TphB with other *cis*-dihydrodiol and non-dihydrodiol dehydrogenases reveals a trend that is closely matched at the phylogenetic level, whereby, despite catalyzing the turnover of a *cis*-dihydrodiol substrate, TphB shares closer homology with dehydrogenases that are active on non-dihydrodiol substrates. Based on our structural data that pertain to the associated metal cofactor, we propose that this trend stems from an obligate requirement for a metal-based catalytic chemistry in case of TphB. *In silico* substrate modeling corroborates our structural finding(s) regarding the putative active site, while providing a compelling mechanistic scheme that involves the Zn^{2+} site, H291, and K295 as key components to perform the required chemistry for catalysis.

Materials and Methods

The chromosomally encoded *tph* gene from *B. xenovorans* LB400 was cloned into pET-28a(+) in frame with an N-terminal hexahistidine tag and expressed in *E. coli* BL21 (DE3) cells. Following purification using nickel affinity chromatography and SEC, crystals of TphB were obtained using the vapor-diffusion method for crystallization (for details, refer to the Supplemental Data). Diffraction data on TphB crystal(s) were collected on a Rigaku R-axis IV++ area detector (home source) while the fluorescent scan for the K-edge for iron and zinc was performed at Stanford Synchrotron Radiation Lightsource, California. Diffraction data were processed using the CCP4 suite of programs.[54] A total of 10 iodide sites were identified and refined using autoSHARP, which resulted in high-quality phases that enabled building and registering of approximately 70% of the backbone using ARP/wARP.[55] The remaining structure was built manually and solvent atoms were selected using Coot[56] and refined with REFMAC[57] to an R_{cryst} of 21.3% and an R_{free} of 26.5%. In total, 187,478 reflections were used in refinement with a sigma cutoff of 2.0. The Ramachandran plot of the refined TphB structure showed good stereochemistry with 94.5% of the residues in the most favored conformations and no residues modeled in disallowed orientations. Overall, 5% of the reflections were set aside for calculation of R_{free}. Data collection statistics are presented in Supplementary Table 1. For *in silico* substrate modeling, residues identified in the crystal structure to project into the putative active site were selected in PyMOL and imported into Spartan '06. Briefly, the amide backbone was maintained for residues where the backbone carbonyl group could conceivably interact with a substrate; remaining residues were trimmed back to the α-carbon for computational efficiency. All non-hydrogen atoms were frozen and the structure was subjected to a semiempirical geometry optimization (PM3) to ensure the correct placement of the hydrogen atoms. An α-hydroxy acid function was built off of the zinc atom and the structure was optimized for the final output after placing selective constraints (refer to the Supplemental Data for detailed methodology regarding substrate modeling).

PDB accession number

Coordinates and structure factors have been deposited in the PDB with accession numbers 4aty and r4atysf, respectively.

Acknowledgements

This work was supported by research grants from the Natural Sciences and Engineering Research Council to M.J.B. and J.E.W. J.B. was supported by a Natural Sciences and Engineering Research Council CGSD fellowship. M.J.B. and J.E.W. are Canada Research Chairs and Michael Smith Foundation for Health Research Scholars. The authors gratefully acknowledge the staff of beamline 9-2 at the Stanford Synchrotron Radiation Lightsource.

Supplementary Data

Supplementary data to this article can be found online at http://dx.doi.org/10.1016/j.jmb.2012.07.022

References

1. Keyser, P., Pujar, B. G., Eaton, R. W. & Ribbons, D. W. (1976). Biodegradation of the phthalates and their esters by bacteria. *Environ. Health Perspect.* **18**, 159–166.
2. Schlafli, H. R., Weiss, M. A., Leisinger, T. & Cook, A. M. (1994). Terephthalate 1,2-dioxygenase system from *Comamonas testosteroni* T-2: purification and some properties of the oxygenase component. *J. Bacteriol.* **176**, 6644–6652.
3. Macarie, H., Noyola, A. & Guyot, J. P. (1992). Anaerobic treatment of a petrochemical wastewater from a terephthalic acid plant. *Water Sci. Technol.* **25**, 223–235.
4. Colborn, T., vom Saal, F. S. & Soto, A. M. (1993). Developmental effects of endocrine-disrupting chemicals in wildlife and humans. *Environ. Health Perspect.* **101**, 378–384.
5. David, R. M., Moore, M. R., Cifone, M. A., Finney, D. C. & Guest, D. (1999). Chronic peroxisome proliferation and hepatomegaly associated with the hepatocellular tumorigenesis of di(2-ethylhexyl)phthalate and the effects of recovery. *Toxicol. Sci.* **50**, 195–205.
6. Ganning, A. E., Brunk, U. & Dallner, G. (1984). Phthalate esters and their effect on the liver. *Hepatology*, **4**, 541–547.
7. Harris, C. A., Henttu, P., Parker, M. G. & Sumpter, J. P. (1997). The estrogenic activity of phthalate esters in vitro. *Environ. Health Perspect.* **105**, 802–811.
8. Huff, J. E. & Kluwe, W. M. (1984). Phthalate esters carcinogenicity in F344/N rats and B6C3F1 mice. *Prog. Clin. Biol. Res.* **141**, 137–154.

9. Jobling, S., Reynolds, T., White, R., Parker, M. G. & Sumpter, J. P. (1995). A variety of environmentally persistent chemicals, including some phthalate plasticizers, are weakly estrogenic. *Environ. Health Perspect.* **103**, 582–587.
10. Kluwe, W. M. (1982). Overview of phthalate ester pharmacokinetics in mammalian species. *Environ. Health Perspect.* **45**, 3–9.
11. Nakai, M., Tabira, Y., Asai, D., Yakabe, Y., Shimyozu, T., Noguchi, M. *et al.* (1999). Binding characteristics of dialkyl phthalates for the estrogen receptor. *Biochem. Biophys. Res. Commun.* **254**, 311–314.
12. Staples, C. A., Parkerton, T. F. & Peterson, D. R. (2000). A risk assessment of selected phthalate esters in North American and Western European surface waters. *Chemosphere*, **40**, 885–891.
13. Ribbons, D. W., Keyser, P., Kunz, D. A., taylor, B. F., Eaton, R. W. & Anderson, B. N. (1984). Microbial degradation of phthalates. In *Microbial Degradation of Organic Compounds* (Gibson, D. T., ed.), pp. 371–397, Dekker, New York.
14. Ribbons, D. W. (1988). More about phthalates. In *Microbial Catabolism and the Carbon Cycle* (Hagedorn, S. R., Hanson, R. S. & Kunz, D. A., eds), pp. 85–100, Harwood, Chur.
15. Cartwright, C. D., Owen, S. A., Thompson, I. P. & Burns, R. G. (2000). Biodegradation of diethyl phthalate in soil by a novel pathway. *FEMS Microbiol. Lett.* **186**, 27–34.
16. Chang, H. K. & Zylstra, G. J. (1998). Novel organization of the genes for phthalate degradation from *Burkholderia cepacia* DBO1. *J. Bacteriol.* **180**, 6529–6537.
17. Gu, J. D., Li, J. & Wang, Y. (2005). Biochemical pathway and degradation of phthalate ester isomers by bacteria. *Water Sci. Technol.* **52**, 241–248.
18. Otsuka, Y., Nakamura, M., Shigehara, K., Sugimura, K., Masai, E., Ohara, S. & Katayama, Y. (2006). Efficient production of 2-pyrone 4,6-dicarboxylic acid as a novel polymer-based material from protocatechuate by microbial function. *Appl. Microbiol. Biotechnol.* **71**, 608–614.
19. Shigehara, K., Y. Katayama, S. Nishikawa, and Y. Hotta. (2001). Polyester and process for producing the same. U.S. patent 6,303,745.
20. Shigehara, K., Y. Katayama, S. Nishikawa, and Y. Hotta. (2002). Polyamide and process for producing the same. U.S. patent 6,340,739.
21. Engelhardt, G., Rast, H. G. & Wallnofer, P. R. (1979). Degradation of aromatic carboxylic acids by *Nocardia* spec DSM 43251. *FEMS Microbiol. Lett.* **5**, 245–251.
22. Karegoudar, T. B. & Pujar, B. G. (1985). Degradation of terephthalic acid by a *Bacillus* species. *FEMS Microbiol. Lett.* **30**, 217–220.
23. Kimura, T. & Ito, Y. (2001). Two bacterial mixed culture systems suitable for degrading terephthalate in wastewater. *J. Biosci. Bioeng.* **91**, 416–418.
24. Sugimori, D., Dake, T. & Nakamura, S. (2000). Microbial degradation of disodium terephthalate by alkaliphilic *Dietzia* sp. strain GS-1. *Biosci. Biotechnol. Biochem.* **64**, 2709–2711.
25. Choi, K. Y., Kim, D., Sul, W. J., Chae, J. C., Zylstra, G. J., Kim, Y. M. & Kim, E. (2005). Molecular and biochemical analysis of phthalate and terephthalate degradation by *Rhodococcus* sp. strain DK17. *FEMS Microbiol. Lett.* **252**, 207–213.
26. Hara, H., Eltis, L. D., Davies, J. E. & Mohn, W. W. (2007). Transcriptomic analysis reveals a bifurcated terephthalate degradation pathway in *Rhodococcus* sp. strain RHA1. *J. Bacteriol.* **189**, 1641–1647.
27. Saller, E. L. H., Schlafioppenberg, H. R. & Cook, A. M. (1995). Purification and some properties of (1*R*,2*S*)-1,2-dihydroxy-3,5-cyclohexadiene-1,4-dicarboxylate dehydrogenase from *Comamonas testosteroni* T-2. *FEMS Microbiol. Lett.* **130**, 97–102.
28. Wang, Y. Z., Zhou, Y. & Zylstra, G. J. (1995). Molecular analysis of isophthalate and terephthalate degradation by *Comamonas testosteroni* YZW-D. *Environ. Health Perspect.* **103**, 9–12.
29. Sasoh, M., Masai, E., Ishibashi, S., Hara, H., Kamimura, N., Miyauchi, K. & Fukuda, M. (2006). Characterization of the terephthalate degradation genes of *Comamonas* sp. strain E6. *Appl. Environ. Microbiol.* **72**, 1825–1832.
30. Shigematsu, T., Yumihara, K., Ueda, Y., Numaguchi, M., Morimura, S. & Kida, K. (2003). *Delftia tsuruhatensis* sp. nov., a terephthalate-assimilating bacterium isolated from activated sludge. *Int. J. Syst. Evol. Microbiol.* **53**, 1479–1483.
31. Chain, P. S., Denef, V. J., Konstantinidis, K. T., Vergez, L. M., Agullo, L., Reyes, V. L. *et al.* (2006). *Burkholderia xenovorans* LB400 harbors a multi-replicon, 9.73-Mbp genome shaped for versatility. *Proc. Natl Acad. Sci. USA*, **103**, 15280–15287.
32. Johnson, G. R., Jain, R. K. & Spain, J. C. (2000). Properties of the trihydroxytoluene oxygenase from *Burkholderia cepacia* R34: an extradiol dioxygenase from the 2,4-dinitrotoluene pathway. *Arch. Microbiol.* **173**, 86–90.
33. Mueller, J. G., Devereux, R., Santavy, D. L., Lantz, S. E., Willis, S. G. & Pritchard, P. H. (1997). Phylogenetic and physiological comparisons of PAH-degrading bacteria from geographically diverse soils. *Antonie Van Leeuwenhoek*, **71**, 329–343.
34. Arnett, C. M., Parales, J. V. & Haddock, J. D. (2000). Influence of chlorine substituents on rates of oxidation of chlorinated biphenyls by the biphenyl dioxygenase of *Burkholderia* sp. strain LB400. *Appl. Environ. Microbiol.* **66**, 2928–2933.
35. Goris, J., De Vos, P., Caballero-Mellado, J., Park, J., Falsen, E., Quensen, J. F., 3rd *et al.* (2004). Classification of the biphenyl- and polychlorinated biphenyl-degrading strain LB400T and relatives as *Burkholderia xenovorans* sp. nov. *Int. J. Syst. Evol. Microbiol.* **54**, 1677–1681.
36. Hubner, A., Danganan, C. E., Xun, L., Chakrabarty, A. M. & Hendrickson, W. (1998). Genes for 2,4,5-trichlorophenoxyacetic acid metabolism in *Burkholderia cepacia* AC1100: characterization of the tftC and tftD genes and locations of the tft operons on multiple replicons. *Appl. Environ. Microbiol.* **64**, 2086–2093.
37. Delano, W. L. (2002). The PyMOL Molecular Graphics System.
38. Gibson, D. T. (1971). The microbial oxidation of aromatic hydrocarbons. *Crit. Rev. Microbiol.* **1**, 199–223.
39. Jerina, D. M., Daly, J. W., Witkop, B., Zaltzman-Nirenberg, P. & Udenfriend, S. (1968). The role of arene oxide-oxepin systems in the metabolism of

aromatic substrates. 3. Formation of 1,2-naphthalene oxide from naphthalene by liver microsomes. *J. Am. Chem. Soc.* **90**, 6525–6527.
40. Oesch, F., Jerina, D. M., Daly, J. W., Lu, A. Y., Kuntzman, R. & Conney, A. H. (1972). A reconstituted microsomal enzyme system that converts naphthalene to *trans*-1,2-dihydroxy-1,2- dihydronaphthalene via naphthalene-1,2-oxide: presence of epoxide hydrase in cytochrome P-450 and P-448 fractions. *Arch. Biochem. Biophys.* **153**, 62–67.
41. Matsuura, K., Hara, A., Deyashiki, Y., Iwasa, H., Kume, T., Ishikura, S. *et al.* (1998). Roles of the C-terminal domains of human dihydrodiol dehydrogenase isoforms in the binding of substrates and modulators: probing with chimaeric enzymes. *Biochem. J.* **336**, 429–436.
42. Terada, T., Fujita, N., Sugihara, Y., Sato, R., Takagi, T. & Maeda, M. (2001). Site-directed mutagenesis studies of bovine liver cytosolic dihydrodiol dehydrogenase: the role of Asp-50, Tyr-55, Lys-84, His-117, Cys-145 and Cys-193 in enzymatic activity. *Chem. Biol. Interact.* **130–132**, 833–845.
43. Hsu, N. Y., Ho, H. C., Chow, K. C., Lin, T. Y., Shih, C. S., Wang, L. S. & Tsai, C. M. (2001). Overexpression of dihydrodiol dehydrogenase as a prognostic marker of non-small cell lung cancer. *Cancer Res.* **61**, 2727–2731.
44. Patel, T. R. & Gibson, D. T. (1974). Purification and propeties of (plus)-*cis*-naphthalene dihydrodiol dehydrogenase of *Pseudomonas putida*. *J. Bacteriol.* **119**, 879–888.
45. Sundlov, J. A., Garringer, J. A., Carney, J. M., Reger, A. S., Drake, E. J., Duax, W. L. & Gulick, A. M. (2006). Determination of the crystal structure of EntA, a 2,3-dihydro-2,3-dihydroxybenzoic acid dehydrogenase from *Escherichia coli*. *Acta Crystallogr., Sect. D: Biol. Crystallogr.* **62**, 734–740.
46. Hulsmeyer, M., Hecht, H. J., Niefind, K., Hofer, B., Eltis, L. D., Timmis, K. N. & Schomburg, D. (1998). Crystal structure of *cis*-biphenyl-2,3-dihydrodiol-2,3-dehydrogenase from a PCB degrader at 2.0 Å resolution. *Protein Sci.* **7**, 1286–1293.
47. Sivaraman, J., Li, Y., Banks, J., Cane, D. E., Matte, A. & Cygler, M. (2003). Crystal structure of *Escherichia coli* PdxA, an enzyme involved in the pyridoxal phosphate biosynthesis pathway. *J. Biol. Chem.* **278**, 43682–43690.
48. Auld, D. S. (2001). Zinc coordination sphere in biochemical zinc sites. *Biometals*, **14**, 271–313.
49. Carbone, V., Hara, A. & El-Kabbani, O. (2008). Structural and functional features of dimeric dihydrodiol dehydrogenase. *Cell. Mol. Life Sci.* **65**, 1464–1474.
50. Patil, D. N., Tomar, S., Sylvestre, M. & Kumar, P. (2010). Expression, purification, crystallization and preliminary crystallographic studies of *cis*-biphenyl-2,3-dihydrodiol-2,3-dehydrogenase from *Pandoraea pnomenusa* B-356. *Acta Crystallogr., Sect. F: Struct. Biol. Cryst. Commun.* **66**, 1517–1520.
51. Holm, L. & Park, J. (2000). DaliLite workbench for protein structure comparison. *Bioinformatics*, **16**, 566–567.
52. Corpet, F. (1988). Multiple sequence alignment with hierarchical clustering. *Nucleic Acids Res.* **16**, 10881–10890.
53. Altschul, S. F., Gish, W., Miller, W., Myers, E. W. & Lipman, D. J. (1990). Basic local alignment search tool. *J. Mol. Biol.* **215**, 403–410.
54. Collaborative Computational Project Number 4. (1994). The CCP4 Suite—programs for protein crystallography. *Acta Crystallogr., Sect. D*, **50**, 760–763.
55. Perrakis, A., Morris, R. & Lamzin, V. S. (1999). Automated protein model building combined with iterative structure refinement. *Nat. Struct. Biol.* **6**, 458–463.
56. Emsley, P. & Cowtan, K. (2004). Coot: model-building tools for molecular graphics. *Acta Crystallogr., Sect. D*, **60**, 2126–2132.
57. Murshudov, G. N., Vagin, A. A. & Dodson, E. J. (1997). Refinement of macromolecular structures by the maximum-likelihood method. *Acta Crystallogr., Sect. D*, **53**, 240–255.